J Mater Sci (2014) 49:8459–8470
DOI 10.1007/s10853-014-8556-x

Temperature-dependent material properties of the components of magnetorheological fluids

Daoming Wang · Bin Zi · Yishan Zeng · Youfu Hou · Qingrui Meng

Received: 20 July 2014 / Accepted: 17 August 2014 / Published online: 27 August 2014

Abstract Material properties of the components of magnetorheological (MR) fluids are critical to their control accuracy and service life. The aim of this study was to reveal the effects of temperature on the material properties of MR fluid components. In this paper, a detailed introduction to the components of MR fluids, including main performance indicators and commonly used materials, was presented at first. Then, theoretical analysis and experimental investigation were performed on the temperature-dependent material properties of MR fluid components. These material properties included the magnetization properties of the magnetic particle, as well as the shear viscosity and thermal expansion of the carrier fluid. Experimental results indicated that both the mass magnetization and coercivity of MR particles decreased as the temperature increased and the phenomenon was particularly obvious at high temperatures. Moreover, an increasing temperature could lead to a severe decrease of the shear viscosity and a relatively large thermal expansion of the carrier fluid. Research results from this study may serve to provide a theoretical and an experimental basis for the preparation of MR fluids with high thermal stability.

Introduction

As a two-phase, multicomponent suspension, the magnetorheological (MR) fluid is mainly composed of micrometer-sized magnetic particles, a non-magnetic carrier liquid and several additional additives [1]. Rheological properties of the fluid, including the yield stress, shear viscosity, and dynamic modulus, all change drastically in the presence of a magnetic field [2–6]. Moreover, the rheological process from a free-flowing state to a solid-like state is rapid and revisable [7–10]. Under a magnetic field, the shear stress of the MR fluid could be continuously and accurately controlled solely by regulating the magnetic intensity. This remarkable feature has given rise to a large variety of engineering applications of the MR fluid in the fields of torque transmission, vibration control, polishing, and shock absorption to enhance the working efficiency and reduce the energy consumption [11, 12]. These application forms include the clutches, brakes, shock absorbers, vehicle suspensions, semi-active vibration dampers, and servo valves [13–19].

In practical applications, the MR fluid mainly operates in three different modes: the shear mode, the valve mode, and the squeeze mode [20–23]. In all cases, the fluid serves as a damping material or transmission medium which may bring about the friction heat due to the frictional interaction among MR particles. This will definitely lead to an increase of the fluid temperature. Since the components of MR fluids are temperature-dependent materials, the increase of temperature will lead to a decrease of the shear stress, in-use thickening or even a complete failure of the MR fluid [24]. As far as we know, material properties of the MR fluid used in an MR actuator are critical to the actuator performance. In particular, the thermal stability of the fluid has a great influence on the working performance, control accuracy, and service life of MR actuators.

For this reason, several relevant works have been performed on the effects of temperature on the performance of MR fluids. Weiss and Duclos [25] measured the viscoelastic properties of an MR fluid (MR-100, Lord Corporation) in the

D. Wang (✉) · B. Zi · Y. Zeng
School of Mechanical and Automotive Engineering, Hefei University of Technology, Hefei 230009, China
e-mail: cumtcmeewdm@hotmail.com

D. Wang · Y. Hou · Q. Meng
School of Mechatronic Engineering, China University of Mining and Technology, Xuzhou 221116, China

temperature range from −40 to 150 °C and found that the plastic viscosity and dynamic yield stress declined by 95 and 10 %, respectively. Bica [26] investigated the electrical conductivity of an MR fluid with a mean particle diameter of 2.1 μm and a volumetric concentration of 30 %. Results showed that the MR fluid became conductive till the magnetic intensity reached 72 kA/m and the electrical conductivity increased by up to 96.8 %, as the temperature increases from 300 to 400 K. Tang et al. [27] experimentally studied on the viscosity–temperature characteristic of an MR fluid and observed that the fluid exhibited an excellent viscosity stability in the temperature range of 20–100 °C. Wiehe et al. [28] performed lots of durability experiments on MR fluids at various temperatures and pointed out that there was a decrease in the lifetime dissipated energy of MR fluids with increasing temperature. Yildirim and Genc [29] researched on the heat transfer of the MR fluid at three different temperature intervals (−20 to 0, 0–50, and 50–100 °C). They found that the thermal conductivity was substantially enhanced for the 50–100°C temperature interval, whereas it showed a decrease in the lower temperature interval from −20 to 0 °C.

As stated above, previous works have been mainly focused on the effects of temperature on MR fluids. However, there are indeed few papers involving the temperature-dependent material properties of the components which are exactly the essential reasons for the temperature dependence of MR fluids. Consequently, the main object of this study is to reveal the effects of temperature on the material properties of the MR fluid components. In terms of the polarization mechanism of the MR fluid, the influence of temperature mainly embodies in the following three aspects: (i) the magnetization properties of the magnetic particle; (ii) the shear viscosity of the carrier fluid; and (iii) the thermal expansion of the carrier fluid.

This paper is organized as follows: "The components of the MR fluid" section gives a detailed introduction to the components of MR fluids; "Magnetization properties of the magnetic particle" section focuses on revealing the effects of temperature on the magnetization properties of the magnetic particle; "Shear viscosity of the carrier fluid" and "Thermal expansion of the carrier fluid" sections discuss the influence of temperature on the shear viscosity and thermal expansion of the carrier fluid, respectively; Sect. 6 gives the conclusions of this paper.

The components of the MR fluid

Magnetic particle

Magnetic polarization of MR particles under field-responsive effect is essential to achieve fluid–solid transition of MR fluids. Therefore, material properties of the particles directly affect the rheological behaviors of MR fluids. In general, a material with high permeability and saturation magnetization and low remnant magnetization and coercivity is a good candidate for MR particulate material. Commonly used materials include Fe, Co, Ni, Fe_3O_4, Fe_3N, carbonyl iron, Fe–Co alloy, and Ni–Fe alloy [30]. Fe–Co and Ni-Fe alloys possess excellent magnetic properties with a saturation magnetization of up to 2.4 T. However, the manufacturing process proves to be complicated and expensive which restricts the wide use of the two materials.

Table 1 Saturation magnetization (at 20 °C) and Curie temperature of several magnetic materials [31, 32]

Material	Saturation magnetization (T)	Curie temperature (°C)
Fe	2.15	770
Co	1.78	1331
Ni	0.605	484
Carbonyl iron	2.23	775
Fe_3Al	0.625	500
Fe–Co alloy	2.4	970

Two factors are usually considered while selecting the MR particulate material: (i) favorable magnetic properties, which are the core factor for the MR effect; (ii) high physical and chemical stability which means that the material should possess an excellent anti-sedimentation stability and a high oxidation resistance. The above two factors mainly depend on the particle material, size, shape, and density. Table 1 shows the saturation magnetization (at 20 °C) and Curie temperature of several magnetic materials.

In practice, the most commonly used material is carbonyl iron powder (CIP) due to its high magnetic permeability, low remnant magnetization, fine particle size, and narrow size distribution, as well as common availability [33]. Generally, CIP is fabricated through the decomposition of iron pentacarbonyl $Fe(CO)_5$. The iron content is 97–99 % and the size distribution range is 0.5–20 μm. Surface morphology of CIP is usually spherical or irregular polygon, and the particle volumetric concentration can reach up to 50 %.

Carrier fluid

The main component of an MR fluid is the carrier fluid which serves as a continuous insulating medium [33]. It also has an important impact on the MR fluid performances. In general, the carrier fluid should possess the following characteristics: (i) a low freezing point and a high boiling point, so as to extend the operating temperature range; (ii) a suitable viscosity. A low viscosity can

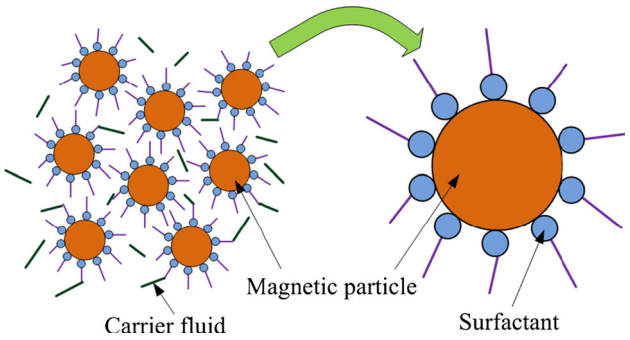

Fig. 1 Schematic diagram of the surfactant

improve the fluidity, while it reduces the anti-sedimentation stability; (iii) high stability, non-flammable, environmentally friendly, and low price.

Typically, there are two kinds of carrier fluid: the non-magnetic carrier fluid and the magnetic carrier fluid. The non-magnetic carrier fluid mainly includes silicone oil, mineral oil, toluene, hydrocarbon oil, water, and ethylene glycol. As far as we know, most commercial MR fluids utilize this kind of carrier fluid. For instance, several commercial MR fluids provided by Load Cooperation, namely MRF-132AD, MRF-241ES, and MRF-336AG, separately use hydrocarbon oil, water, and silicone oil as the carrier fluid. As for the magnetic carrier fluid, it refers to the magnetic fluid with nano-sized particles (typically about 10 nm) [34]. Such fluid can improve the shear yield stress and the anti-sedimentation stability. However, it is seldom used because it significantly reduces the regulation range of the shear stress.

At present, a widely used carrier fluid is the silicone oil due to its wide operating temperature range, strong anti-oxidation ability, high flash point, and low volatility. The silicone oil is a colorless and transparent synthetic polymer material. It has a pour point of lower than −60 °C, a flash point ranging from 200 to 300 °C, and a thermal decomposition temperature of up to 400 °C.

Additive

Additional additives are required for the MR fluid to improve the material performances. Usually, the amount of additives used in the MR fluid is less than 5%. There are many kinds of additives, such as surfactant, stabilizer, and lubricant.

Surfactant is an oligomer that consists of both hydrophilic and lipophilic groups. It is usually capable of interacting with both the carrier fluid and the particles. One end of the surfactant is composed of several non-polar hydrocarbon chains and the other end is usually a polar group, such as carboxylic acid, sulfuric acid, amino, or amino group. As shown in Fig. 1, the hydrophilic end adsorbs on the particle surface, while the lipophilic end swings in the carrier fluid, which can prevent particle sedimentation and improve the polarization ability of MR particles effectively.

Stabilizer serves to keep the MR particles suspending stably in the carrier fluid. It is able to form a sub-particle group between the particles and the carrier fluid, which makes the MR fluid in a gel state to avoid particle agglomeration and thereby increases the anti-sedimentation stability.

Lubricant is used to improve the lubrication effect between MR particles. A good lubrication can reduce the particle adhesion, so as to enhance the dispersion uniformity of MR particles in the carrier fluid.

Additive selection for MR fluids should take the following two points into consideration: (i) a good intermiscibility with the carrier fluid and a strong affinity with the MR particles, so as to acquire an excellent anti-sedimentation stability; (ii) a broad operating temperature range and a high thermal stability in order to avoid thermal decomposition. Commonly used additives for MR fluids include oleic acid, polyethylene glycol, polysorbate 80, silica gel, coupling agent, nano-sized magnesium lithium silicate, and other nonionic additives.

Magnetization properties of the magnetic particle

Theoretical analysis

Magnetic susceptibility is a physical quantity used to measure the magnetization performance of a material. It is equal to the ratio of magnetization to the magnetic intensity, which is expressed as

$$\chi = \frac{M}{H}, \tag{1}$$

where M is the magnetization and H is the magnetic intensity.

The MR particulate material is typically a ferromagnetic material with temperature-dependent magnetic properties [35]. Spontaneous magnetization of the particles decreases as the temperature increases. Once the temperature reaches up to the Curie temperature of the material, the spontaneous magnetization reduces to zero. As a result, the material translates from ferromagnetic state into superparamagnetic state. The temperature-dependent magnetic susceptibility $\chi(T)$ follows the Curie–Weiss law described as

$$\chi(T) = \frac{C}{T - T_c}, \tag{2}$$

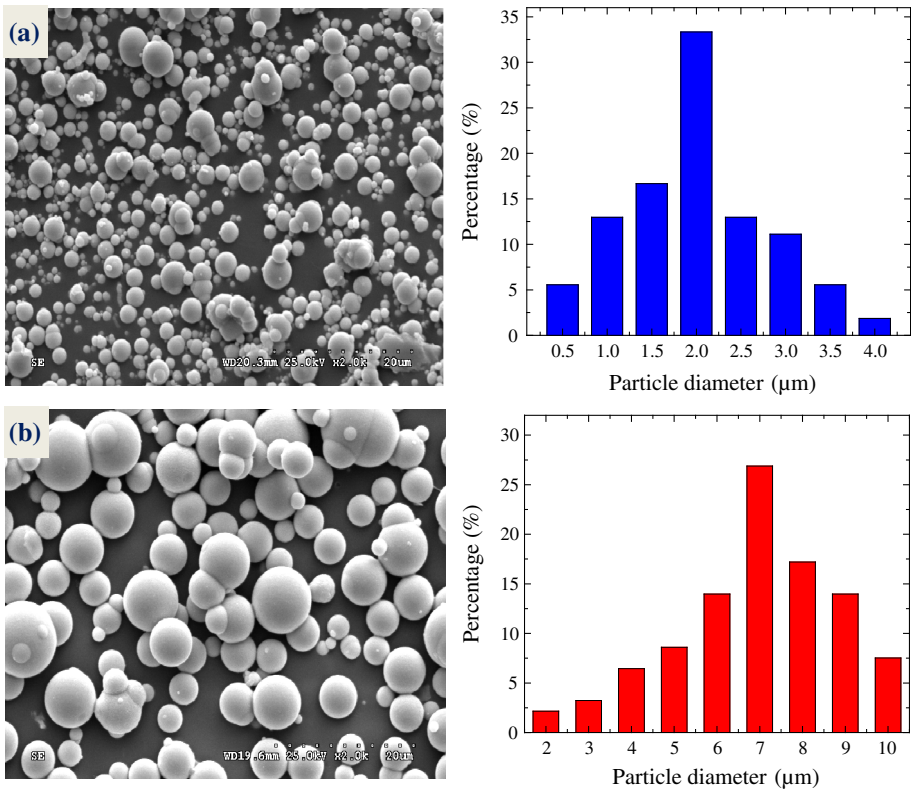

Fig. 2 SEM images and size distributions of two types of CIP: **a** TJ1; **b** TJ2

where C is the Curie constant, T is the absolute temperature, and T_c the Curie temperature of the material.

In the magnetization process, the magnetization increases with the magnetic intensity at first. Then, the increasing rate gradually slows down until the magnetization reaches the saturation state. The corresponding stable magnetization is known as the saturation magnetization. For ferromagnetic materials, the relationship between saturation magnetization and temperature (below the Curie temperature) follows the Bloch's law given as [36, 37]

$$M_s(T) = M_0\left[1 - \left(\frac{T}{T_c}\right)^{\alpha}\right], \tag{3}$$

where $M_s(T)$ is the temperature-dependent saturation magnetization, M_0 is the saturation magnetization at 0 K, and α is the Bloch's exponent depending on the material structure and composition.

For the single-domain magnetic particles with uniaxial anisotropy, the temperature-dependent coercivity $H_c(T)$ below the superparamagnetic blocking temperature follows the Kneller's law described as [38]

$$H_c(T) = H_0\left[1 - \left(\frac{T}{T_B}\right)^{1/2}\right], \tag{4}$$

where H_0 is the coercivity at 0 K and T_B is the superparamagnetic blocking temperature.

As discussed above, the magnetization properties of MR particles, including the magnetic susceptibility, saturation magnetization, and coercivity, are all affected by the temperature. Therefore, the following experiments were conducted to reveal the influence laws of temperature on the above-mentioned magnetization properties.

Experimental apparatus

Two types of CIP with different particle sizes, model TJ1 and TJ2, were selected in this study. They were provided by China Jiangsu Tianyi Superfine Metal Powder Co., Ltd. The appearance of CIP is dark gray and its compaction density is about 7.86 g/cm^3 [39, 40]. Surface morphology of two types of CIP was observed with a scanning electron microscope (SEM) and the SEM images and size distributions were shown in Fig. 2.

It is visible in Fig. 2 that most of the particles appear regular spherical in shape and basically separate from each other. Moreover, the two types of particles both have a narrow size distribution. To be specific, TJ1 has a particle diameter range of 0.5–4.0 μm with a mean diameter of about 2 μm, and the diameter of TJ2 varies from 2 to 10 μm with an average value of nearly 7 μm. However, there is still a little reunion phenomenon among the particles due to the large specific surface area which brings about a great van der Waals forces of attraction between

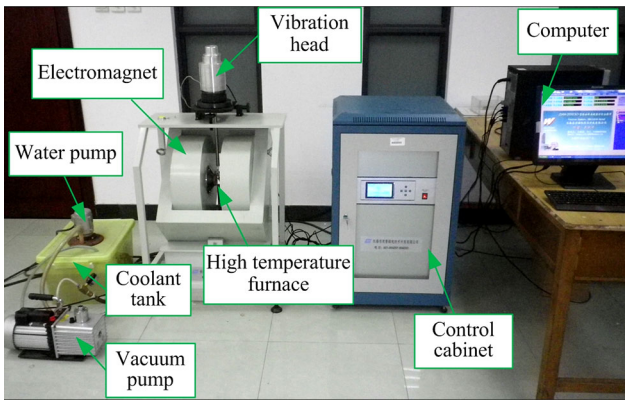

Fig. 3 JDAW-2000D VSM

the particles. Thus, an appropriate surface treatment is needed for the chosen CIP to avoid particle agglomeration and improve the anti-sedimentation stability.

Vibrating sample magnetometer (VSM) is a high-sensitive instrument for the magnetic moment measurement of a sample material. It is based on the principle of electromagnetic induction. The magnetic moment is calculated from the detected induction voltage caused by the coil vibration. The VSM can be used for the measurement of magnetization curve (*M–H* curve), magnetic hysteresis loop, demagnetization curve, and magnetization–temperature curve (*M–T* curve). It has many advantages, such as a rapid and simple measuring process, a high sensitivity and accuracy, as well as a user-friendly interface.

Magnetization measurements of CIP were conducted with a VSM (model JDAW-2000D) from China Changchun INPRO Magnetoelectric Technology Co., Ltd. As shown in Fig. 3, the VSM is composed of a vibration head, an electromagnet, a water pump, a coolant tank, a high-temperature furnace, a vacuum pump, a control cabinet, and a computer. The control cabinet comprises an electromagnet power supply controlled by AT89C52 microprocessor, a vibration source, as well as a magnetic field, and a temperature measurement unit. Main parameters of JDAW-2000D VSM are given as follows: magnetic moment range (10^{-3}–300 emu), temperature range (−145 to 770 K), magnetic intensity range (0–1280 kA/m), temperature precision (±1.5 K), and relative precision (≤1%).

Results and discussion

Room temperature condition

Magnetic hysteresis loop and magnetization curve (*M–H* curve) are two important indicators for evaluating the magnetic properties of materials. Several magnetic parameters, including magnetic permeability μ, saturation magnetization M_s, remnant magnetization M_r, and coercivity H_c, are available from the two curves.

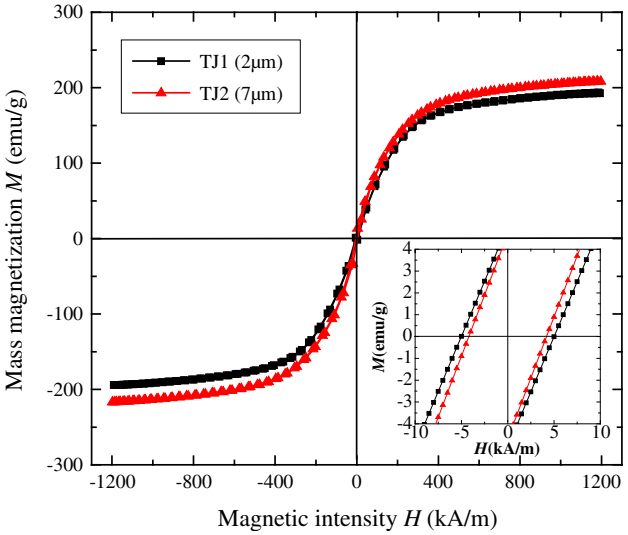

Fig. 4 Magnetic hysteresis loops of CIP at RT

Figure 4 indicates the magnetic hysteresis loops of two kinds of CIP (2 and 7 μm) at room temperature (RT). The inset of the figure shows a magnified region around the origin to make the coercivity more visible.

It is observed in Fig. 4 that the CIP presents excellent soft magnetic properties at RT. The hysteresis loop is very smooth and no obvious hysteresis phenomenon appears. Therefore, it is an ideal choice for MR particulate material. Furthermore, the saturation mass magnetization and coercivity of TJ1 are respectively 194.3 emu/g and 5.0 kA/m, while these of TJ2 are up to 204.2 emu/g and only 4.3 kA/m, respectively. It is obvious that the CIP with a larger particle diameter exhibits a greater saturation magnetization and a lower coercivity. This phenomenon can be explained by the fact that the ratio of regularly arranged atomic structures increases with the particle size which leads to an increase of magnetic moment for per unit mass CIP.

M–H curve indicates the nonlinear relationship between magnetization *M* and magnetic intensity *H*. In the experiment, *M–H* curves of two kinds of CIP (2 and 7 μm) at RT were measured as shown in Fig. 5. The mass magnetization increases sharply with the magnetic intensity at the beginning. In particular, the increasing trend appears to be almost linear in the magnetic intensity range from 0 to 150 kA/m. Then, it gradually slows down with a further increase of the magnetic intensity. When *H* increases to a certain value, *M* gradually stabilizes and the stable value is known as the saturation mass magnetization. Similar to that shown in Fig. 4, the CIP with a larger particle size presents a greater saturation mass magnetization.

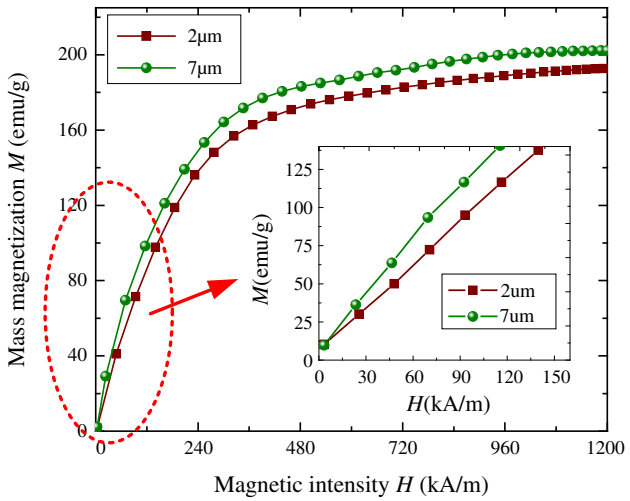

Fig. 5 *M–H* curves of CIP at RT

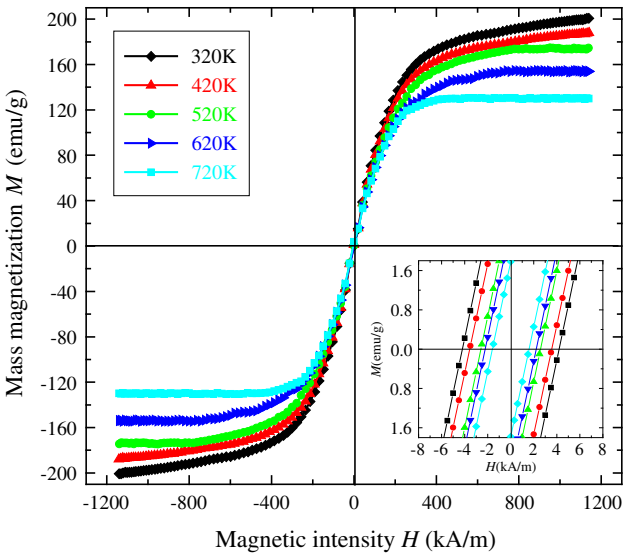

Fig. 6 Magnetic hysteresis loops of CIP at various temperatures

For the MR fluid, the shear yield stress increases with the saturation magnetization, while the magnetizing power and hysteresis loss decrease with the coercivity [41]. Therefore, the CIP with a larger particle size is better for the MR fluid to improve the magnetization properties. However, a server problem will emerge on increasing the particle size. The off-field viscosity increases and the anti-sedimentation stability becomes worse, which in return reduces the rheological behavior and even service life of the MR fluid. Therefore, the particle size selection is an important issue which should combine with the specific requirements for MR fluids in practice.

High-temperature condition

As discussed in "Theoretical analysis" section, the temperature has a great influence on the magnetization properties of materials. For this reason, the following tests were conducted under high-temperature conditions to explore the effects of temperature on the magnetization properties of CIP. In the experiments, the particle diameter of CIP sample is 7 μm and the sample mass is 41.2 mg.

Magnetic hysteresis loops of CIP at various temperatures were initially measured as presented in Fig. 6. In the measurements, the magnetic intensity range is 0–1200kA/m and the temperature is 320, 420, 520, 620, and 720 K, respectively. It is obvious in Fig. 6 that a certain degree of magnetization performance degradation occurs in the CIP under high-temperature conditions. The mass magnetization reduces with the increasing temperature under the same magnetic intensity. This phenomenon is mainly attributed to the fact that the temperature rise accelerates the atomic motion and thereby disorders the magnetic moment orientation of the particles, which resulting in a reduction in the magnetic moment of per unit mass CIP. In more detail, as the temperature rises from 320 to 420 K, the saturation mass magnetization decreases from 198.8 to 187.2 emu/g, a reduction of 11.6 emu/g. However, the reduction reaches up to 25.8 emu/g as the temperature increases from 620 to 720 K. Thus, we can conclude that the decreasing rate of the mass magnetization also increases with the temperature.

In addition, the coercivity of CIP could be calculated from the magnetic hysteresis loops. Experimental results of the coercivity at various temperatures were plotted in Fig. 7. Combining with the experimental data, a fitting equation of the coercivity which decreases as a function of temperature was obtained as well. Also, the fitting curve was presented in Fig. 7. Obviously, in the figure, the coercivity appears a decreasing trend with the increase of temperature. As the temperature varies from 320 to 720 K, the reduction ratio of the coercivity reaches about 90.5 %. The phenomenon is mainly due to the thermal fluctuation of the blocking moment induced by the anisotropy barrier. Furthermore, the experimental results fit very well to the Kneller's law given in Eq. (4) and the coercivity of CIP at 0 K is obtained as $H_0 = 12.1$ kA/m, while the superparamagnetic blocking temperature is $T_B = 718.7$ K.

Magnetization–temperature curve (*M–T* curve) refers to the relationship between magnetization and temperature, which can visually reflect the variation law of magnetization with temperature. Figure 8 illustrates the *M–T* curve of CIP in the temperature range from 320 to 720 K. In the experiment, the magnetic intensity is 1200 kA/m and the temperature varies from 320 to 720 K in increments of 10 K.

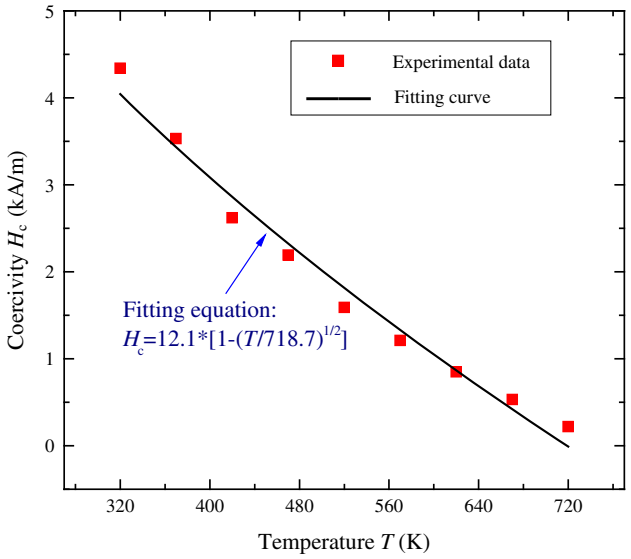

Fig. 7 Coercivity as a function of temperature in the range of 320–720 K

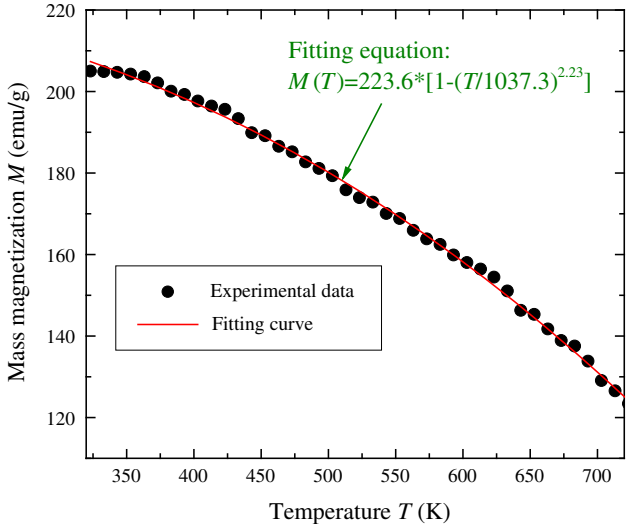

Fig. 8 *M–T* curve of CIP in the temperature range from 320 to 720 K

As shown in Fig. 8, the mass magnetization decreases with the increase of temperature and the decreasing trend becomes sharp at a high temperature. Specifically, as the temperature increases from 320 to 720 K, the mass magnetization decreases from 203.2 to 124.8 emu/g, a decrease of 78.4 emu/g which accounts for about 38.5 % of the mass magnetization at 320 K. Consequently, it is concluded that the temperature has a great influence on the magnetization properties of CIP and the effect is more obvious at high temperatures.

Besides, the nonlinear relationship between mass magnetization and temperature was numerically fitted using a

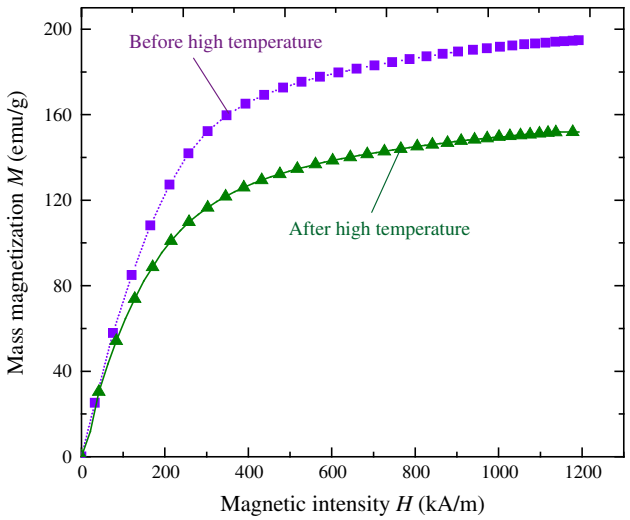

Fig. 9 *M–H* curves of CIP exposed before/after high temperature at RT

nonlinear fitting method based on the Bloch's law in Eq. (3). The fitting equation and curve were also plotted in Fig. 8. Referring to the fitting equation, the saturation mass magnetization at absolute zero M_0, the Curie temperature T_c, and the Bloch's exponent α of CIP were respectively obtained as 223.6 emu/g, 1037.3 K, and 2.23.

M–H curves of CIP exposed before/after high temperature at RT were measured as depicted in Fig. 9. In the experiments, one CIP sample was exposed to a high temperature up to 770 K for about 50 min. It is apparent in Fig. 9 that the magnetization properties decline significantly after a long-term exposure to high-temperature environment. In detail, the saturation mass magnetization reduces from 204.2 to 159.8 emu/g, a reduction ratio of about 21.74 %. This phenomenon is mainly attributed to the formation of oxidation layer on the particle surface, which in return leads to a reduction of the particle magnetism.

As known to us, sufficient thermostability at high temperature is required for a commercial MR fluid in industrial and engineering applications [42]. Therefore, a thermalgravimetric analysis (TGA) was performed on the CIP to evaluate the antioxidant property in a high-temperature environment. The experiment was conducted in the temperature range from 25 to 800 °C with a heating rate of 50 °C. And the thermalgravimetric curve of CIP in the air environment was obtained as shown in Fig. 10. The CIP exhibits an excellent antioxidant property in the temperature below 300 °C. It indicates that the CIP can fully meet the temperature requirements for MR fluids in torque transmission applications, which usually have an operating temperature of less than 300 °C. However, once the temperature exceeds 300 °C, an obvious oxidation phenomenon occurs at

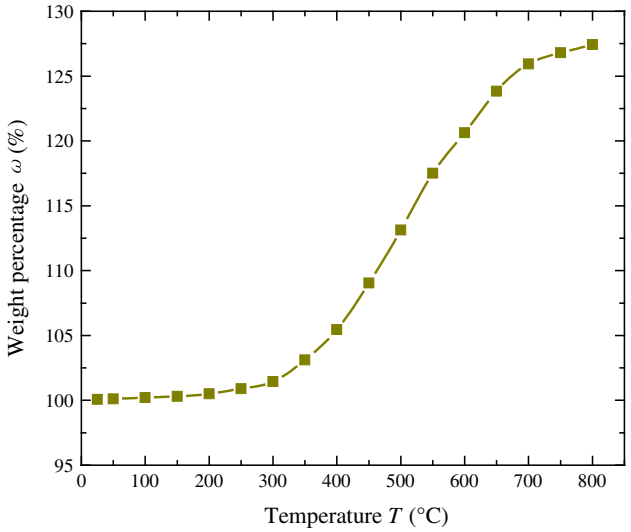

Fig. 10 Thermalgravimetric curve of CIP in the air environment from 25 to 800 °C

the CIP and the sample weight increases sharply in the temperature range from 300 to 550 °C. As the temperature continues to increase, the oxide layer becomes thicker and thicker and the increasing trend in weight percentage gradually slows down. At 800 °C, the weight percentage of the CIP reaches up to 127.4 %.

Shear viscosity of the carrier fluid

Theoretical study

Shear viscosity is a physical quantity used to measure the viscous characteristics of liquids, which is also known as viscosity coefficient, proportion coefficient, and viscous damping coefficient. Referring to Newton's inner friction law, it is equal to the ratio of shear stress to velocity gradient described as

$$\mu = \frac{\tau}{\mathrm{d}u/\mathrm{d}y}, \tag{5}$$

where τ is the shear stress per unit area and $\mathrm{d}u/\mathrm{d}y$ the velocity gradient.

Based on the basic theory of fluid mechanics, the relationship between shear viscosity and kinematic viscosity is given by

$$\mu = \rho\upsilon, \tag{6}$$

where υ is the kinematic viscosity and ρ the density of the fluid.

The shear viscosity of the carrier fluid has a great influence on MR fluid performances. Usually, the anti-sedimentation stability increases with the shear viscosity. However, a large viscosity may lead to a reduction of the regulation range of the shear stress. On the contrary, the decrease of shear viscosity can increase the regulation range, whereas it reduces the anti-sedimentation stability. For either Newtonian or non-Newtonian fluids, the viscosity varies with temperature and the viscosity–temperature characteristics can be described by the Arrhenius equation as

$$\mu = A\mathrm{e}^{(E_\mathrm{a}/RT)}, \tag{7}$$

where A is the pre-exponential factor which is a constant, E_a is the flow activation energy, R is the molar gas constant, $R = 8.314$ J/(mol K), and T the thermodynamic temperature.

Referring to Eq. (7), the sensitivity of viscosity to temperature is measured by the flow activation energy. It refers to the required energy for the molecules to overcome while entering into the molecular clearances. Generally, the viscosity is more sensitive to temperature variation as the flow activation energy increases.

The logarithmic transformation of Eq. (7) on both sides is written as

$$\ln\mu = \ln A + \frac{E_\mathrm{a}}{\mathrm{R}T}. \tag{8}$$

It is concluded from the analysis that the shear viscosity of the carrier liquid is affected by temperature. Moreover, a temperature increase will definitely occur in the MR fluid whether in the shear mode, valve mode, or squeeze mode. This will affect the output characteristic and control accuracy of MR actuators. Therefore, it is necessary to perform the experimental investigation on the viscosity–temperature characteristics of the carrier liquid.

Experimental investigation

Viscosity–temperature measurements of the carrier fluid were carried out with a kinematic viscosity meter (KVM) from China Dalian North Analysis Apparatus Factory. As shown in Fig. 11, the KVM is mainly composed of a ring heater, a blender, a thermostatic bath, a thermometer, a display panel, and several capillary viscometers. Main parameters of BF-03A KVM are given in Table 2.

As a widely used carrier fluid for MR fluids, the methyl silicone oil (MSO) was selected in the experiments. Moreover, two types of MSO, namely 50# and 100#, were used for a comparative analysis. Kinematic viscosities of 50# MSO and 100# MSO were measured from 25 to 100 °C. Besides, the density of silicon oil also decreased as a function of temperature and it was tested as well. Measuring data concerning the kinematic viscosity and the density at each temperature were presented in Table 3.

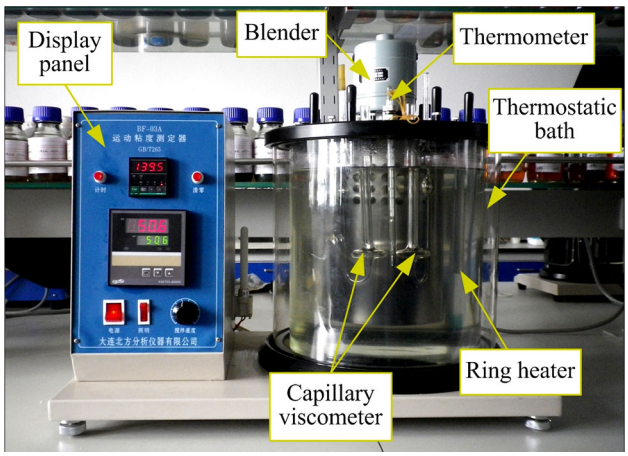

Fig. 11 BF-03A KVM

Table 2 Main parameters of BF-03A KVM

Parameter	Value/range
Applicable object	Transparent Newton fluid
Capillary viscometer	Ostwald-Pinkevich type
Bath hole number	4
Temperature range	RT ~100°C
Temperature precision	±0.1 °C

Table 3 Kinematic viscosities and densities of MSO at different temperatures

Temperature (°C)	Kinematic viscosity (mm^2/s)		Density (kg/m^3)	
	50#	100#	50#	100#
25	49.15	98.36	960.2	964.4
30	41.28	83.97	953.2	957.4
40	39.34	77.05	947.6	951.7
50	33.75	65.47	941.2	945.5
60	28.87	56.01	933.5	937.8
70	25.05	48.55	926.1	930.3
80	21.88	42.07	915.7	919.9
90	19.17	36.75	905.7	909.8
100	16.64	32.01	896.0	900.1

Combining with the experimental results in Table 3, the shear viscosities of MSO at different temperatures were calculated based on Eq. (6). The viscosity–temperature curves were plotted in Fig. 12. It is visible that the viscosities for two types of MSO both decrease with the increase of temperature. At the beginning, the decreasing rate is relatively rapid which is followed by a gradual declining trend. In more detail, as the temperature increases from 25 to 100 °C, the shear viscosity of 50# MSO and

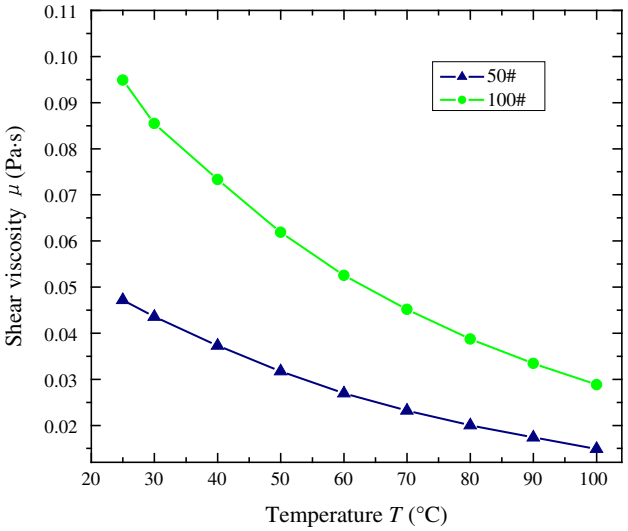

Fig. 12 Viscosity–temperature curves of MSO

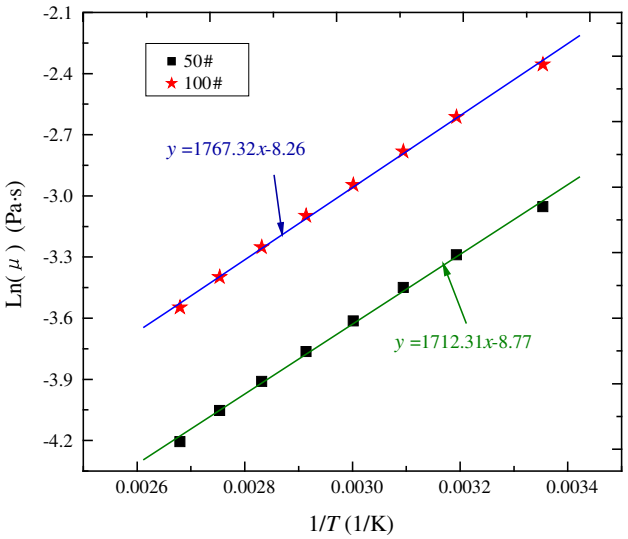

Fig. 13 Variation curves between ln μ and $1/T$

100# MSO decreases by 0.0323 and 0.0661 Pa s, respectively, a reduction of about 67.4 and 69.6 %. Additionally, the viscosity index is calculated as 433 for 50# MSO and 422 for 100# MSO. Therefore, a carrier fluid with low shear viscosity is better for the MR fluid to improve the viscosity–temperature stability.

As described in Eq. (8), the pre-exponential factor A is a constant. Thus, there is a linear relationship between ln μ and $1/T$. The linear constant is equal to the ratio of flow activation energy E_a to molar gas constant R. Based on the experimental data in Table 3, variation curves between ln μ and $1/T$ were obtained with the linear fitting method

as shown in Fig. 13. With reference to Fig. 13 and Eq. (8), the flow activation energy E_a for 50# MSO and 100# MSO was calculated as 14.24 and 14.69 kJ, respectively. It is visible that the flow activation energy increases with the fluid viscosity. As a consequence, we should choose a carried fluid with low flow activation energy to achieve a good thermal stability.

Thermal expansion of the carrier fluid

Thermal expansion refers to the phenomenon that the geometric property of a material increases with temperature under a certain pressure. It can be measured by the thermal expansion coefficient which is also regarded as an important indicator to assess the thermal stability of a material. In general, there are three types of thermal expansion coefficient: cubic expansion coefficient, superficial expansion coefficient, and linear expansion coefficient. The cubic expansion coefficient refers to the relative increase of volume with a temperature increment of 1 K. For most fluids, the cubic expansion coefficient α_v is relatively small which can be expressed as

$$\alpha_v = \frac{V_2 - V_1}{V_1(T_2 - T_1)}, \tag{9}$$

where V_1 and V_2 are the fluid volumes at the temperatures of T_1 and T_2, respectively.

Table 4 Cubic expansion coefficients of several liquids

Liquid	Cubic expansion coefficient (10^{-3}/°C)
Water	0.21
Ethylene glycol	0.57
Glycerol	0.52
Dimethylbenzene	0.85
Kerosene	1

Table 4 shows the cubic expansion coefficients of several liquids at 20 °C.

In the experiment, a vacuum drying oven (VDO), model DZF-6021, from China Shanghai Zhongyou Instrument Co., Ltd, was used for the temperature control of the carrier liquid. A photograph of the VDO was shown in Fig. 14. The VDO possesses a temperature control range from RT + 10 to 250 °C with a temperature fluctuation of ±1°C. Through the measurements of fluid volumes at various temperatures, the cubic expansion coefficient could be calculated in accordance with Eq. (9).

Two types of MSO (50# and 100#) with an initial volume of 30 mL were separately poured into two transparent tubes and then be placed in the VDO. Thereafter, the volumes of MSO at various temperatures were obtained by regulating the controlled temperature of VDO. Furthermore, the thermal expansion coefficient could be calculated referring to Eq. (9). In the experiment, the controlled temperature ranges from 30 to 250 °C in increments of 20 °C. Experimental results concerning the thermal expansion characteristics of MSO at various temperatures were depicted in Fig. 15.

In Fig. 15, the volume scales up almost proportionally to the temperature in the range from 30 to 250 °C. Moreover,

Fig. 14 DZF-6021 VDO

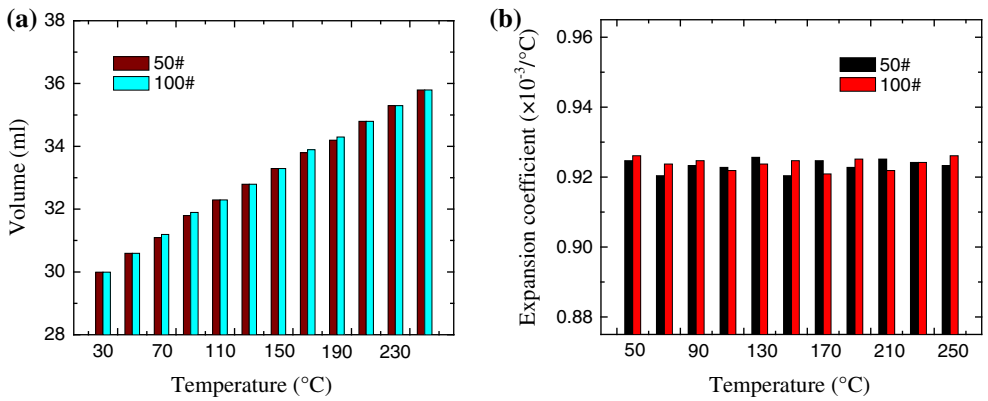

Fig. 15 Thermal expansion characteristics of MSO at various temperatures: **a** volume; **b** expansion coefficient

the phenomenon presents basically the same between the two types of MSO. Thus, it is found that the fluid viscosity does not affect the thermal expansion characteristic. The volume of 50# MSO increases from 30 to 35.8 mL in the temperature range from 30 to 250 °C, an expansion ratio of nearly 19.3 %. Meanwhile, in the same temperature range, the thermal expansion coefficient remains basically unchanged with a value of about 0.924×10^{-3}/°C. Comparing with several commonly used carrier fluids in Table 4, such as water, ethylene glycol, and dimethylbenzene, the thermal expansion coefficient of MSO is relatively large. It can easily lead to an overpressure phenomenon in the confined cavity. Therefore, the seals with high pressure capacity are required in the design of MR actuators to prevent fluid leakage.

Conclusions

This study presented a comprehensive study on the temperature-dependent material properties of the components of MR fluids by means of theoretical analysis and experimental investigation. The results concerning the magnetization properties of MR particles as well as the shear viscosity and thermal expansion of the carrier fluid were presented and discussed. They reveal that the saturation magnetization and coercivity of MR particles decrease by 38.5 and 90.5 % with an increasing temperature from 320 to 720 K, respectively. In addition, the magnetization performance of MR particles declines sharply after a long-term exposure to high-temperature environment due to the formation of surface oxidation layer. Moreover, the shear viscosity of the carrier fluid decreases as the temperature increases, and a carrier fluid with a higher viscosity is more sensitive to the temperature variation. In practice, a carrier fluid with low activation energy is required to improve the thermal stability of MR fluids. Furthermore, the temperature increase can lead to a relatively large thermal expansion of MSO in comparison with several commonly used carrier fluids, such as water, ethylene glycol, and dimethylbenzene. The thermal expansion coefficient remains basically unchanged with a value of about 0.924×10^{-3}/°C. It may lead to an overpressure phenomenon in the confined cavity where the MR fluid is stored. As a consequence, the seals with high pressure capacity are needed in the MR actuator design to prevent fluid leakage.

Acknowledgements This work was supported by the National Natural Science Foundation of China (No. 50975275 and 51075386) and the Fundamental Research Funds for the Central Universities (2014HGCH0015). Meanwhile, the authors deeply appreciate the insightful comments and valuable suggestions from anonymous referees and editors for improving the quality of our paper.

References

1. Boczkowska A, Awietjan SF, Wejrzanowski T, Kurzydlowski KJ (2009) Image analysis of the microstructure of magnetorheological elastomers. J Mater Sci 44:3135–3140. doi:10.1007/s10853-009-3417-8
2. Jolly MR, Bender JW, Carlson DJ (1999) Properties and applications of commercial magnetorheological fluids. J Intell Mater Syst Struct 10:5–13
3. Mazlan SA, Ekreem NB, Olabi AG (2007) The performance of magnetorheological fluid in squeeze mode. Smart Mater Struct 16:1678–1682
4. Senkal D, Gurocak H (2010) Serpentine flux path for high torque MRF brakes in haptics applications. Mechatronics 20:377–383
5. Molazemi M, Shokrollahi H, Hashemi B (2013) The investigation of the compression and tension behavior of the cobalt ferrite magnetorheological fluids synthesized by co-precipitation. J Magn Magn Mater 346:107–112
6. Nguyen PB, Choi SB (2013) Accurate torque control of a bi-directional magneto-rheological actuator considering hysteresis and friction effects. Smart Mater Struct 22:055002
7. Mazlan SA, Issa A, Chowdhury HA, Olabi AG (2009) Magnetic circuit design for the squeeze mode experiments on magneto-rheological fluids. Mater Des 30:1985–1993
8. Li WH, Du H, Chen G, Yeo SH, Guo N (2003) Nonlinear viscoelastic properties of MR fluids under large-amplitude-oscillatory-shear. Rheol Acta 42:280–286
9. Park EJ, Stoikov D, Falcao da Luz L, Suleman A (2006) A performance evaluation of an automotive magnetorheological brake design with a sliding mode controller. Mechatronics 16:405–416
10. Kim SY, Kwon SH, Liu YD, Lee JS, You CY, Choi HJ (2014) Core–shell-structured cross-linked poly(glycidyl methacrylate)-coated carbonyl iron microspheres and their magnetorheology. J Mater Sci 49:1345–1352. doi:10.1007/s10853-013-7818-3
11. Jang KI, Nam E, Lee CY, Seok J, Min BK (2013) Mechanism of synergetic material removal by electrochemomechanical magnetorheological polishing. Int J Mach Tool Manu 70:88–92
12. Sim HH, Kwon SH, Choi HJ (2013) Xanthan gum-coated soft magnetic carbonyl iron composite particles and their magneto-rheology. Colloid Polym Sci 291:963–969
13. Liu B, Li WH, Kosasih PB, Zhang XZ (2006) Development of an MR-brake-based haptic device. Smart Mater Struct 15:1960–1966
14. Sung KG, Choi SB (2008) Effect of an electromagnetically optimized magnetorheological damper on vehicle suspension control performance. P I Mech Eng D: J Aut 222:2307–2319
15. Senkal D, Gurocak H (2009) Spherical brake with MR fluid as multi degree of freedom actuator for haptics. J Intell Mater Syst Struct 20:2149–2160
16. Erol O, Gurocak H (2011) Interactive design optimization of magnetorheological-brake actuators using the Taguchi method. Smart Mater Struct 20:105027
17. Wang D, Hou Y (2013) Design and experimental evaluation of a multidisk magnetorheological fluid actuator. J Intell Mater Syst Struct 24:640–650
18. Ha SH, Seong MS, Choi SB (2013) Design and vibration control of military vehicle suspension system using magnetorheological damper and disc spring. Smart Mater Struct 22:065006
19. Imaduddin F, Mazlan SA, Rahman MAA, Zamzuri H, Ichwan B (2014) A high performance magnetorheological valve with a meandering flow path. Smart Mater Struct 23:065017
20. Carlson JD, Jolly MR (2000) MR fluid, foam and elastomer devices. Mechatronics 10:555–569
21. Boelter R, Janocha H (1997) Design rules for MR fluid actuator in different working modes. In: Proceedings of the SPIE's 1997

Symposium on Smart Structures and Materials, San Diego, United States, vol 3045, pp 148–159
22. Olabi AG, Grunwald A (2007) Design and application of magneto-rheological fluid. Mater Des 28:2658–2664
23. Imaduddin F, Mazlan SA, Zamzuri H (2013) A design and modeling review of rotary magnetorheological damper. Mater Des 51:575–591
24. Shah K, Upadhyay RV, Aswal VK (2012) Influence of large size magnetic particles on the magneto-viscous properties of ferrofluid. Smart Mater Struct 21:075005
25. Weiss KD, Duclos TG (1994) Controllable fluids: the temperature dependence of post-yield properties. Int J Mod Phys B 8: 3015–3032
26. Bica I (2006) The influence of temperature and of a longitudinal magnetic field upon the electrical conductivity of magnetorheological suspensions. Phys Rev B 371:145–148
27. Tang L, Yue E, Luo SA, Zhao GM, Zhang P, Zhang DY, Yang BL (2011) Study on temperature performance of magnetorheological fluid. J Funct Mater 42:1065–1067
28. Wiehe A, Kieburg C, Maas J (2013) Temperature induced effects on the durability of MR fluids. J Phys Conf Ser 412:012017
29. Yildirim G, Genc S (2013) Experimental study on heat transfer of the magnetorheological fluids. Smart Mater Struct 22:085001
30. Pu HT, Jiang FJ (2005) Research progress and application of magnetorheological fluids. Chem Ind Eng Prog 24:132–136
31. Wang AR, Xu G, Shu CJ (2010) Magnetic fluid and its application. Xi-an Jiao Tong University Press, Xi-an
32. Jang KI, Seok J, Min BK, Lee SJ (2009) Behavioral model for magnetorheological fluid under a magnetic field using Lekner summation method. J Magn Magn Mater 321:1167–1176
33. Ashour O, Rogers CA, Kordonsky W (1996) Magnetorheological fluids: materials, characterization, and devices. J Intell Mater Syst Struct 7:123–130
34. Rosensweig RE (1985) Ferrohydrodynamics. Cambridge University Press, New York
35. Karakoc K, Park EJ, Suleman A (2008) Design considerations for an automotive magnetorheological brake. Mechatronics 18:434–447
36. Hendriksen PV, Linderoth S, Lindgård PA (1993) Finite-size modifications of the magnetic properties of clusters. Phys Rev B 48:7259–7273
37. Demortiere A, Panissod P, Pichon BP, Pourroy G, Guillon D, Donnio B, Bégin-Colin S (2011) Size-dependent properties of magnetic iron oxide nanocrystals. Nanoscale 3:225–232
38. Maaz K, Mumtaz A, Hasanain SK, Bertinoc MF (2010) Temperature dependent coercivity and magnetization of nickel ferrite nanoparticles. J Magn Magn Mater 322:2199–2202
39. Cho MS, Lim ST, Jang IB, Choi HJ, Jhon MS (2004) Encapsulation of spherical iron-particle with PMMA and its magnetorheological particles. IEEE T Magn 40:3036–3038
40. Zhou Y, Jerrams S, Chen L (2013) Multi-axial fatigue in magnetorheological elastomers using bubble inflation. Mater Des 50:68–71
41. Shi XG (2010) Research on sedimentation stability and rheological properties of reduced iron MRF. M.S. Dissertation. Northeastern University, Shenyang
42. Liu YD, Choi HJ, Choi SB (2012) Controllable fabrication of silica encapsulated soft magnetic microspheres with enhanced oxidation-resistance and their rheology under magnetic field. Colloids Surf A 403:133–138